# LANGMUIR

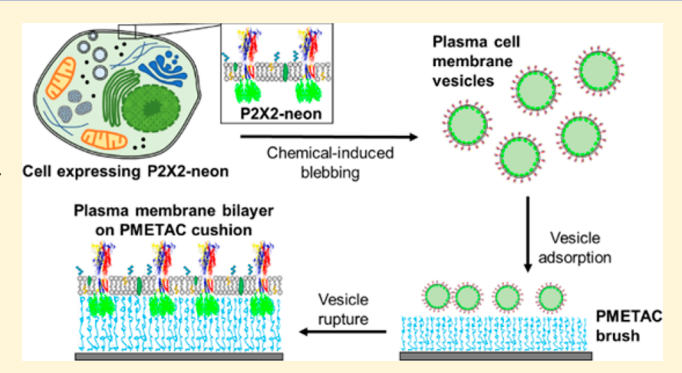
### Biologically Complex Planar Cell Plasma Membranes Supported on Polyelectrolyte Cushions Enhance Transmembrane Protein Mobility and Retain Native Orientation

Han-Yuan Liu, †, § Wei-Liang Chen, †, § Christopher K. Ober, † and Susan Daniel\*, †

<sup>†</sup>Robert F. Smith School of Chemical and Biomolecular Engineering, <sup>‡</sup>Department of Material Science and Engineering, Cornell University, Ithaca, New York 14853, United States

Supporting Information

ABSTRACT: Reconstituted supported lipid bilayers (SLB) are widely used as in vitro cell-surface models because they are compatible with a variety of surface-based analytical techniques. However, one of the challenges of using SLBs as a model of the cell surface is the limited complexity in membrane composition, including the incorporation of transmembrane proteins and lipid diversity that may impact the activity of those proteins. Additionally, it is challenging to preserve the transmembrane protein native orientation, function, and mobility in SLBs. Here, we leverage the interaction between cell plasma membrane vesicles and polyelectrolyte brushes to create planar bilayers from cell plasma membrane vesicles that have budded from the cell



surface. This approach promotes the direct incorporation of membrane proteins and other species into the planar bilayer without using detergent or reconstitution and preserves membrane constituents. Furthermore, the structure of the polyelectrolyte brush serves as a cushion between the planar bilayer and rigid supporting surface, limiting the interaction of the cytosolic domains of membrane proteins with this surface. Single particle tracking was used to analyze the motion of GPI-linked yellow fluorescent proteins (GPI-YFP) and neon-green fused transmembrane P2X2 receptors (P2X2-neon) and shows that this platform retains over 75% mobility of multipass transmembrane proteins in its native membrane environment. An enzyme accessibility assay confirmed that the protein orientation is preserved and results in the extracellular domain facing toward the bulk phase and the cytosolic side facing the support. Because the platform presented here retains the complexity of the cell plasma membrane and preserves protein orientation and mobility, it is a better representative mimic of native cell surfaces, which may find many applications in biological assays aimed at understanding cell membrane phenomena.

#### 1. INTRODUCTION

Mammalian cell membranes are composed of lipids, cholesterol, glycans, and proteins. These biological membranes serve as a selectively permeable barrier that encases the cell cytosolic components and defines organelles. Proteins embedded in these membranes are essential for a variety of cellular functions, such as sensing and interacting with the local environment, signaling and communication with other cells,<sup>2</sup> transporting of material into and out of compartments,<sup>3</sup> and performing crucial enzymatic activities.4 The structure, function, and activity of these protein is highly dependent on the local lipid environment and often specific allosteric species being present. 5,6

Supported lipid bilayers (SLBs) are widely employed as model systems for investigating the function of membrane proteins, their dependence on protein-lipid interactions, and myriad biotechnology applications ranging from biosensing to bioseparation. Lately, these platforms have become a popular tool for studies of virus-host interactions, peptide penetration, and cell membrane phenomena because their planar geometry is compatible with surface-based analytical tools such as variable angle epifluorescence microscopy (VAEM), 10-12 total internal reflection microscopy (TIRF), 13,14 atomic force microscopy (AFM), 15,16 and quartz crystal microbalance (QCM). 17 For such studies to provide the maximum insight from experiments, it is imperative that the SLB be the truest representation of the entire plasma membrane surface as possible. However, the most significant challenges of this platform have been incorporating properly oriented, mobile transmembrane proteins into SLBs and capturing the complex plasma membrane lipid milieu. The most prevalent alternative, detergent-based extraction, and reconstitution method, suffers from the possibility that the detergent may alter the protein structure and native lipid-

Special Issue: Early Career Authors in Fundamental Colloid and Interface Science

Received: August 18, 2017 Revised: October 7, 2017 Published: October 11, 2017



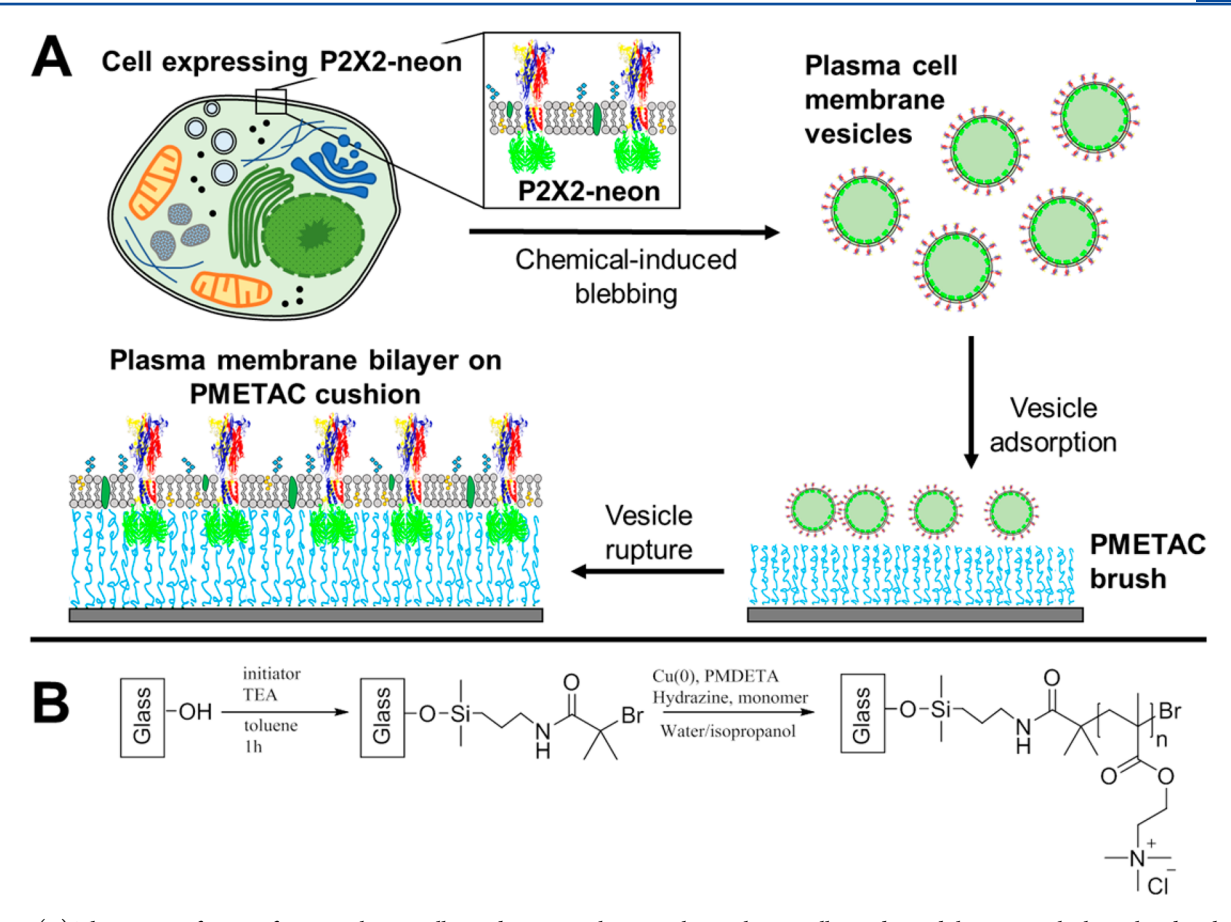


**Figure 1.** (A) The strategy for transforming plasma cell membrane vesicles into planar plasma cell membrane bilayer on polyelectrolyte brushes. The P2X2-neon protein structure is based on P2X4 structure solved by Kawate et al.<sup>50</sup> After the bilayer is formed, the polymer continues to swell and expand (not drawn to scale here). (B) Synthesis of the polymer brushes starting with immobilization of the initiator on the glass slides, and surface initiated polymerization of PMETAC, as described in more detail in the Materials and Methods section.

protein interactions, and orientations of species are scrambled. 18

To create a closer biomimetic of cell membranes in this planar geometry, our laboratory has established methods for the creation of supported, planar bilayers out of plasma cell membrane vesicles, also referred to as cell blebs, which bud from the plasma membrane surface. Such blebs are essentially small biopsies of the intact plasma membrane surface that are readily generated either by mechanical cell lysis and centrifugation methods 19,20 or chemically induced methods.<sup>21-23</sup> However, these methods are not the only ones available to create biologically complex plasma vesicles and supported bilayers. In a previous study, Tanaka et al.<sup>24</sup> demonstrated the deposition of human erythrocyte membranes on planar surfaces coated with thin polymer films by using the human erythrocyte ghosts. Simonsson et al.<sup>25</sup> employed a hydrodynamically driven edge of a SLB to rupture an adsorbed cell membrane vesicle to incorporate membrane species into the merged SLB. Later, Pace et al. 26 demonstrated another way to incorporate the transmembrane proteins and membrane species into SLBs by mixing vesicles made from synthetic lipids (PEGylated lipids and POPC lipids) with cell plasma membrane vesicles.

We learned early on in our initial studies that cell plasma membrane vesicles formed by the chemical induction method typically do not spontaneously rupture to form support planar bilayers when presented with standard SLB-compatible surfaces, like glass and silicon, without being stimulated by

some means. In our previous works, 7,27 we showed that these types of cell plasma membrane vesicles adsorbed to glass will rupture into planar sheets during the adsorption and spontaneous rupture of synthetic "fusogenic" liposomes. However, while the native orientation of proteins is preserved using this method of formation, we found that (not surprisingly) the space beneath the planar supported bilayer is not enough to accommodate the protein cytosolic parts, thus they become immobilized in this platform. One approach that we have used to increase protein mobility in these platforms is to use PEGylated liposomes to both induce bleb rupture and provide some space between the glass surface and the lower leaflet of the planar bilayer to accommodate the proteinaceous cytosolic extensions. By this approach, we have been able to achieve  $\sim$ 53% mobility of a 6-pass  $\alpha$  helix transmembrane protein called P2X2.22

While this is among some of the best TMP mobility statistics for supported bilayers in complex membrane compositions, the drawbacks still remains that only about half of proteins are mobile and that the planar bilayer is now "diluted" with extra lipids from the fusogenic liposomes, resulting in a hybrid mixture of synthetic and native membranes. Here, we employ a strategy that leverages the electrostatic interaction between a tunable-length polyelectrolyte brush, poly([(2-methacryloyloxy)ethyl]trimethylammonium chloride) (PME-TAC), and charged plasma cell membrane vesicles to spontaneously form a biologically complex planar supported cell membrane without using any synthetic fusogenic lip-

osomes, while also preserving native protein orientation and gaining a significantly higher mobile fraction of proteins.

Brief Perspective on Polymer Cushions As Bilayer Supports. In the pioneering work of McConnell et al. <sup>28,29</sup> SLBs were first shown to spontaneously form on solid substrates (e.g., glass/quartz/silicon) by vesicle fusion resulting in a thin (~1 nm) lubricating layer of water between the SLB and supporting surface. <sup>30</sup> This limited space is too small to avoid the interaction between the hard wall and the SLB, thus making mobile protein integration difficult without introducing some spacers or cushions. Tethered polymer cushions have been placed beneath SLBs using various strategies to lift it from the support while preserving its structural integrity. <sup>31,32</sup> By manipulation of charge/hydrophilicity/chemical structure of the cushioning polymer, plenty of proteins have been reconstituted successfully with varying levels of mobility and apparent functionality in these systems. <sup>27,33–37</sup>

With the advance of synthetic chemistry, polymer brushes featuring dense surface tethering, and consequently an extended structure, have been used as both cushions and a functional material. 38,39 For example, functional polymer brushes can exhibit additional properties like being stimuliresponsive, <sup>40</sup> antifouling/repellant, <sup>41</sup> and serve as biosensing materials. <sup>42</sup> These properties can also benefit the study of SLBs, for example, functional polymer brushes have been used as cushions in recent years leading to the definition of several design rules for brush cushion properties. Smith et al.<sup>35</sup> is the first example of applying polyacrylamide brushes as SLB cushions and the conclusion of the study suggested that the optimal condition for SLB quality is a trade-off between maximizing thickness, which reduces interfacial interaction, and minimizing roughness of the brushes, which increases defects in the brush layer. Later, it was shown that, by incorporation of responsive monomers, either pH/thermal responsive brush cushions could be used to actively control the height of the SLB without adversely affecting its mobility. 43,44 On the other hand, Santonicola et al.45 showed that SLB formation was not successful on zwitterionic poly[2-(N-3-sulfopropyl-N,Ndimethylammonium)ethyl methacrylate] brushes when the swollen thickness was higher than 35 nm. These studies suggested that beyond this thickness, additional driving forces are needed to rupture the vesicles since the vesicle-glass interaction is too weak at these distances. Blakeston et al. 46 directly compared the formation of SLB on zwitterionic or anionic polymer brushes and also concluded that electrostatic attraction between vesicle and polymer promotes vesicle rupture. They also showed that for zwitterionic brushes containing cysteine groups, where the zeta potential was ca. -10 mV, oppositely charged vesicles could rupture and form SLBs, retaining some mobility on them. However, no mobility was observed when vesicles remained unruptured on the polyelectrolyte brush or when the electrostatic attraction between SLBs and the polyelectrolyte brush was too strong.

In this work, PMETAC brushes, which are composed of positively charged monomers, are extremely hydrophilic, <sup>47,48</sup> and have been shown to be biocompatible, <sup>39,49</sup> are chosen as polymer cushions for supported bilayers, but uniquely here, these supported bilayers are not made from reconstituted lipids and proteins, but directly from cell plasma membrane blebs. The permanent affiliated positive charges of the polymer induce rupture of naturally negatively charged cell plasma membrane vesicles, and the swelling of polymer chains over time creates a space between the planar bilayer and glass substrate (Figure 1)

on the order of several hundred nanometers or more. These PMETAC brush cushions prevent the interaction of extramembranous domains of membrane proteins with the glass support and drastically increase the mobility of transmembrane proteins expressed in this system.

#### 2. MATERIALS AND METHODS

**2.1. Materials.** Allylamine, anhydrous toluene, chlorodimethylsilane, hydrazine, hydrochloric acid, inhibitor remover (for removing hydroquinone and monomethyl ether hydroquinone), magnesium sulfate, [2-methacryloyloxy)ethyl]trimethylammonium chloride (80% in water) (METAC), Pt on activated carbon (10 wt %), N,N,N,N,N,N-pentamethyldiethylenetriamine (PMDETA), and anhydrous trimethylamine (TEA) were purchased from Sigma-Aldrich and used without purification unless stated otherwise. METAC was passed through inhibitor remover to remove the inhibitor before use. Copper tape (882-L COPPER) with 88.9  $\mu$ m copper film was from Lamart Co. All the other solvents were purchased from Fisher Scientific. Cantilevers were purchased from Applied NanoStructures, Inc. (ACCESS-NC) and Olympus Corporation (OMCL-TR400PB).

**2.2. Synthesis of PMETAC Brushes.** First, 2-bromo-2-methyl-Nallylpropanamide was synthesized by published procedure and used as a subsequent reactant. 51 Next, hydrosilylation with chlorodimethylsilane was carried out using another literature procedure to obtain monofunctional ATRP initiator, 2-bromo-2-methyl-N-{3-[chloro-(dimethyl)silyl]-propyl}propanamide. 51,52 Glass slides were cleaned in the solution made of 70% (v/v) H2O, 15% (v/v) HCl (ACS reagent, 37%) and 15% H<sub>2</sub>O<sub>2</sub> (ACS reagent, 30%) at 50 °C for an hour. Subsequently they were washed repetitively with methanol and toluene and dried with nitrogen. Moisture was further removed by 10 min 110 °C oven baking. Glass slides were then oxidized using a Harrick Plasma Cleaner for 7 min. In a glovebox, the glass slides pieces were immersed in a toluene solution of the initiator (10 mM) and TEA (0.5 mM) for an hour at room temperature. The substrates were then removed from the solution and washed with methanol and toluene sequentially. Initiator-tethered glass slides were then blown dry under nitrogen gas.

Polymerization was conducted by first preparing the setup as shown in the literature. Sa Glass slide was cut into pieces with the size corresponding to the initiator-deposited piece. A glass piece was then coated with copper tape to be the catalyst source. This taped glass piece was then clamped face-to-face together with initiator-deposited glass slides by a copper clamp. The distance between the pieces was separated by Teflon spacer with d=0.5 mm. The setup was then put into a solution of 16 mL METAC, 16 mL DI water, 8 mL isopropanol, 288  $\mu$ L PMDETA, and 12  $\mu$ L hydrazine, and polymerization was conducted at room temperature for a given time. Afterward, the glass slides were removed from the solution and rinsed with iced DI water and isopropanol before being blown dry with nitrogen gas.

**2.3. Characterization of PMETAC Brushes.** Polymer brushes were characterized by Asylum MFP-3D atomic force microscopy (AFM). The thickness of the brushes was determined by comparing the height with a scratched (polymer removed) area. The dry topography was characterized with AC tapping mode and silicon cantilevers (model: ACCESS-NC). The wet topography was characterized with contact mode with nominal force constant of 0.02 N/m, and the applied force was set below 3 nN to define the interface. Silicon nitride cantilevers with a gold tip-side coating and a gold/chromium reflex coating (model: OMCL-TR400PB) were used for wet topography.

**2.4. Cells and Plasmids.** BHK cells are widely used for stable expression of recombinant proteins and the study of biological process. BHK cells used here were obtained from the American Type Culture Collection (ATCC) and grown in Dulbecco's modified Eagle medium (DMEM) (CellGro) supplemented with 10% fetal bovine serum (Gibco), 100 U/ml penicillin and 10  $\mu$ g/mL streptomycin (CellGro), 1% HEPES buffer (CellGro). The pYFP-GPI-N1 plasmid was generous gift from the Baird/Holowka research group at Cornell University and used for transfection of BHK cells to express a

glycophosphatidylinositol (GPI) anchored yellow fluorescent (YFP) protein. The pINR3-Neon-THR-P2X2 plasmid mentioned in previous study<sup>27</sup> was the generous gift from the Kawate research group at Cornell University and generated by using a standard molecular biology technique to insert a full length mouse P2X2 receptor followed by a thrombin cleavage site (Gly-Leu-Val-Pro-Arg-Gly) between *Bam*HI and XhoI in pINR3 vector. BHK cells were used to express this neon green fused transmembrane P2X2 receptor.

- **2.5. Preparation of PEGylated Liposomes.** 1-Oleoyl-2-palmitoyl-sn-glycero-3-phosphocholine (POPC) and 1,2-dipalmitoyl-sn-glycero-3-phosphoethanolamine-N-[methoxy(polyethylene glycol)-5000] (PEG5000-PE) were used in this experiment. Both are purchased from Avanti Polar Lipids. In the experiments, 99.5% POPC 0.5% PEG5000-PE, were used to conduct the experiment. The lipid mixture was in chloroform, and a stream of nitrogen was used to evaporate the chloroform solvent gently. To ensure full evaporation, the lipid films were stored under the vacuum for 3 h to remove the residual chloroform. To create vesicles, phosphate buffered saline (PBS) buffer (5 mM NaH<sub>2</sub>PO<sub>4</sub>, 5 mM Na<sub>2</sub>HPO<sub>4</sub>, 150 mM NaCl at pH 7.4) was added to the dried films to the concentration of 2 mg/mL. Single unilamellar liposomes were prepared by extrusion using a 50 nm membrane (Nucleopore Polycarbonate, GE Health) with at least 15 passes.
- **2.6.** Preparation of Plasma Cell Membrane Vesicles.  $9 \times 10^5$  BHK cells were seeded in 10 cm culture dishes (Corning) and grew for 24 h in a 37 °C, 5% CO<sub>2</sub> incubator. 18  $\mu$ L of Turbofect transfection reagent (ThermoScientific) and 6  $\mu$ g of DNA plasmid, pYFP-GPI-N1 or pINR3-Neon-THR-P2X2, were used in the transfection process for each plate and incubated with BHK cells for 24 h in a 37 °C, 5% CO<sub>2</sub> incubator. After the transfection process, the cells were washed with GPMV buffer (2 mM CaCl<sub>2</sub>, 10 mM HEPES, 150 mM NaCl at pH 7.4). Blebbing solution, 4 mL of GPMV buffer with 25 mM formaldehyde (FA) and 2 mM dithiothreitol (DTT) (0.075%FA), was added to induce cell bleb formation and release. The cells were incubated in the blebbing solution for 2 h at 37 °C. After incubation for 2 h at 37 °C, cell blebs were settled on ice for 15 min to separate cell debris and plasma cell membrane vesicles were collected from the supernatant.
- 2.7. Characterization Size, Charge, and Concentration of Cell Plasma Membrane Vesicles. Nanoparticle tracking analysis (NTA, Nanosight NS300, Malvern) was used to determine the size and concentration of blebs in the supernatant. Laser Doppler electrophoresis (Zetasizer Nano ZS, Malvern) was used to measure the zeta-potential of blebs. For measurement of zeta-potential, cell plasma membrane vesicles were measured in GPMV buffer.
- **2.8.** Preparation for planar plasma membrane bilayer formation. Polydimethylsiloxane (PDMS) wells were made with elastomer/cross-linker mixture of Sylgard 184 (Robert McKeown Company). A 10:1 (elastomer:cross-linker) mixture of Sylgard 184 was mixed and baked in the oven for 3 h at 78 °C. After curing into PDMS sheets, wells were punched out with diameters of  $\sim$ 1 cm. These PDMS wells were attached to the PMETAC brush glass slides. Then, 200  $\mu$ L of solution containing plasma cell membrane vesicles at approximately 5 × 10<sup>8</sup> blebs/mL was added into the well and incubated for 50 min. This time was chosen to allow an excess of time for bilayer formation and polymer swelling. After the plasma membrane bilayer formed, the well was gently rinsed with GPMV buffer to remove the excess plasma cell membrane vesicles.

For PEGylated planar plasma membrane bilayer formation, PDMS wells were attached to the dry clean glass slides (25  $\times$  25 mm No.1.5, VWR). The glass slides were pretreated by piranha solution (70% (v/v)  $\rm H_2SO_4$  (BDH) and 30% (v/v)  $\rm H_2O_2$  (Sigma 50 wt %)) for 10 min and rinsed by flushing DI water 20 min continuously. Then 100  $\mu L$  of solution containing blebs at approximately 5  $\times$  10 $^8$  blebs/mL was added into the well and incubated for 15 min. After incubation, the well was rinsed gently with PBS buffer to remove the unattached blebs. Then, 100  $\mu L$  of PEGylated liposomes at 2 mg/mL was added into the well and incubated for 30 min to form the bleb bilayer. After the bleb bilayer formed, the well was rinsed with PBS buffer again to remove the excess liposomes.

- 2.9. Fluorescence Recovery after Photobleaching (FRAP) for Bilayer Characterization. In order to verify the formation of the plasma membrane bilayer, Octadecyl Rhodamine B chloride (R18, Molecular Probes), a membrane intercalating fluorophore, was used to label the cell vesicle membranes. In the labeling process, 200  $\mu L$  cell membrane vesicle solution was incubated with 1 µL 0.36 mM R18, dissolved in ethanol, for 15 min in a sonicating bath (VWR). Nonintegrated R18 was removed by using a G25 spin column (GE Healthcare) before incubating vesicles in the PDMS well. R18 labeling allows visual observation of the state of vesicles, as either punctate fluorescence spots, indicting intact vesicles, or diffuse fluorescence intensity, indicating rupture has occurred and the fluorophores are able to freely diffuse in the 2-D plane of the resultant bilayer. After the bilayers formed (or not), images were recorded by inverted Zeiss Axio Observer.Z1 microscope with  $\alpha$  Plan-Apochromat 20× objectives. R18 also served as a probe for lipid diffusion and mobile fraction by FRAP. A 20  $\mu$ m diameter spot in bilayer was bleached by 150 mW 561 nm optically pumped semiconductor laser (Coherent, Inc.) for 200 ms. The recovery of the bleached spot was monitored for 15 min and the fluorescence intensity of the spot was determined and normalized in each image. The data of fluorescence intensity was fit with a Bessel function following the method of Soumpasis et al.<sup>54</sup> and then the following equation,  $D = w^2/4t_{1/2}$ , where w is the full width at halfmaximum of the Gaussian profile of the focused beam, was used to calculate the diffusion coefficient.
- **2.10.** Enzyme Accessibility Assays for Characterization of Protein Orientation in Planar Cell Membrane Bilayer. 300 U/mL of thrombin (Sigma) was used to examine the accessibility of N-terminal Neon domain of P2X2-neon and 100  $\mu$ g/mL Proteinase K (Ambion) was used to examine the accessibility of YFP domain of GPI-YFP in the bilayer. For determination of protein orientation in plasma membrane bilayer, 100  $\mu$ L of proteinase K or thrombin was added to the well containing the formed plasma membrane bilayer. Images were recorded in TIRF mode at a 10 min interval to track the change in fluorescent signals. As the enzyme cleaves the fluorescent domain of the proteins, the domain leaves the evanescent field and results in the loss of fluorescent signals in the bleb bilayer within the evanescent wave. Fluorescent signals were quantified by particle counting. The number of fluorescent particles was compared to the control experiments without adding enzyme.
- 2.11. Characterization of Motion of Individual Membrane Proteins by Single Particle Tracking. A variety of methods for single particle tracking (SPT) have already been reported in previous literature. 55-58 To enable accurate tracking, all the trajectories were found and calculated by using the single particle tracking method previously reported in the literature.  $^{27}$  This method identified the particle location by their intensity, change of intensity from previous frame, and displacement from previous frame to find the match for every trajectory.<sup>59</sup> Only particle trajectories that last for at least 20 frames were used in the analysis. A particle that only moves around inside an immobile fluorescent area between images is regarded as immobile.<sup>58</sup> The single particle tracking algorithm uses the initial slope of the mean squared displacement (MSD) from the first three time steps to determine the local homogeneous diffusion coefficient. 60,61 To access and quantify the mobility, we employ moment scaling spectrum (MSS) analysis reported by previous literature<sup>58,62</sup> to objectively quantify the mobility of a particle via a parameter denoted as  $\beta$ . Here,  $\beta$  describes the type of motion for each particle.  $\beta$  < 0.4 is confined diffusion;  $0.4 \le \beta \le 0.6$  is quasi-free diffusion;  $\beta > 0.6$  is convective diffusion. For thick cushions exceeding the evanescent wave height, variable angle epifluorescence microscopy (VAEM) was used for imaging. For other cases, total internal reflection microscopy (TIRF) was used to track and image the fluorescent protein, either P2X2-neon or GPI-YFP. The settings and operation of microscope are described later. All the images were analyzed by using Matlab (Mathworks) and ImageJ (NIH).
- **2.12.** Microscope Settings and Operation. VAEM and TIRF microscopy were also applied to conduct the experiments of protein orientation and single particle tracking for protein motion on an inverted Zeiss Axio Observer.Z1 microscope with an  $\alpha$  Plan-

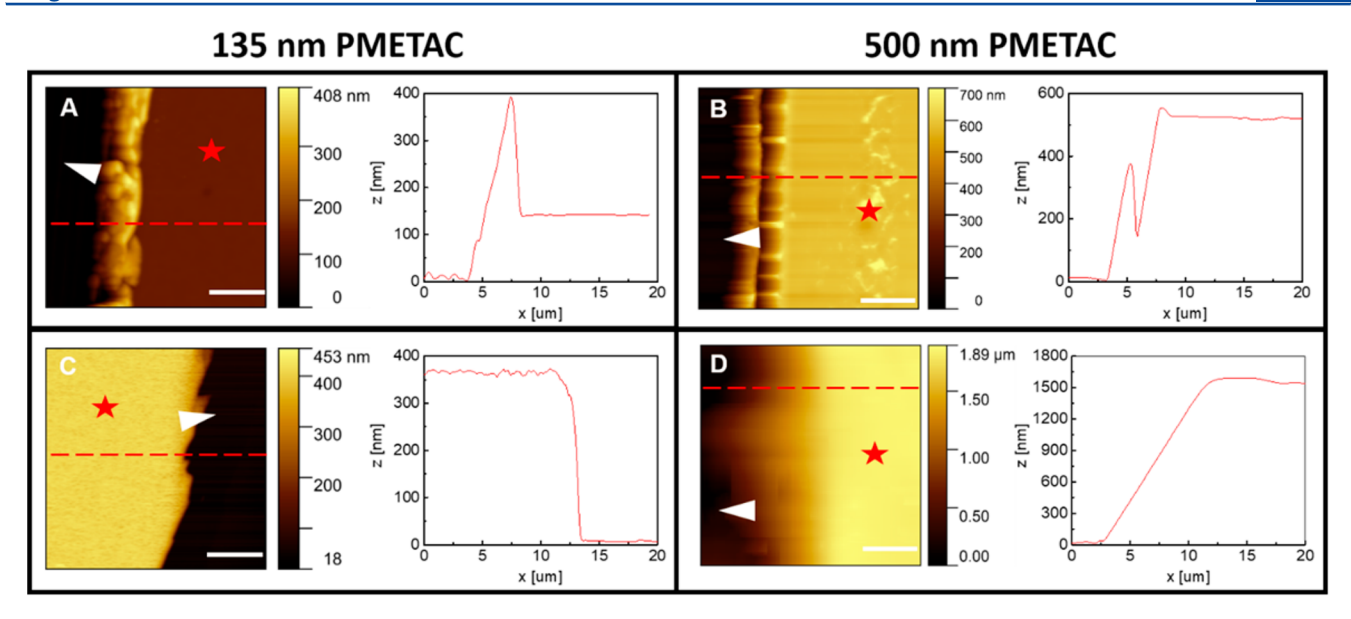


Figure 2. Topography of PMETAC brushes grafted on glass slides as measured by AFM. (A) Dry topography of "thin brush" with,  $d_{\rm dry}=135.2\pm17.221$  nm. (B) Dry topography of "thick brush",  $d_{\rm dry}=499.2\pm30.654$  nm. (C) Wet topography of "thin brush",  $d_{\rm wet}=367.9\pm14.342$  nm. (D) Wet topography of "thick brush"  $d_{\rm wet}=1.627\pm0.0965$  μm. White arrows indicate the position of the scratch. Red stars indicate the location of PMETAC brush. Each image size is  $20\times20$  μm² with a 5 μm scale bar shown in white. The height profile (red dashed line) distinguishes the bare glass surface from the polymer brush.

Apochromat 100× objective. 488 and 561 nm wavelength from solidstate lasers were used to excite the sample. A Laser TIRF 3 slider (Carl Zeiss, Inc.) was used to control angle. The excitation light was filtered by Semrock LF488-B-ZHE filter cube and sent to an electron multiplying CCD camera (ImageEM C9100-13, Hamamatsu).

#### 3. RESULTS AND DISCUSSION

3.1. Characterization of PMETAC Brush. Polymer brushes were synthesized by surface-initiated Cu(0)-meditated living radical polymerization on initiator deposited glass slides. Compared to the traditional atom-transfer radical polymerization technique, this approach has advantages in terms of its oxygen tolerance, activation rate, and end-group fidelity. 63,64 PMETAC brushes with different thickness were fabricated by changing polymerization time and characterized with AFM. It was found empirically that PMETAC brushes much thinner than 135 nm (dry) resulted in poor mobility in bilayers, so we choose to examine thoroughly brushes of two sizes (135 and 500 nm, dry state) in a series of tests to probe the properties of planar bilayers formed on them. In the following sections, the thinner PMETAC brushes are named "135 nm PMETAC brushes" while the thicker brushes were named by "500 nm PMETAC brushes". The dry topography of two PMETAC brushes of these thicknesses are shown in Figure 2A,B. The thickness was derived by comparing the brush height against a scratched area where the polymer was removed (Figure 2A,B, white arrows). In both cases, no defect or surface aggregation of the polymer was observed and the surface roughness (rootmean-square value) in the dry state for both thicknesses was found to be  $3.921 \pm 2.935$  nm for the shorter brush and 6.152 $\pm$  0.531 nm for the longer brush.

Wet polymer topography was also measured by AFM in the same GPMV buffer solution used as the aqueous media for the planar bilayer formation in the subsequent experiments to determine the swollen thickness of the cushion that will reside under the planar bilayer (Figure 2C,D). The wet thicknesses of the PMETAC brushes were found to be  $\sim$ 3 times higher than

that of the dry state. However, in the buffer, the surface roughnesses were similar. For the 135 nm PMETAC brush, it was  $7.045 \pm 1.643$  nm, and for the 500 nm PMETAC brush it was  $7.497 \pm 1.393$  nm. The bilayer quality formed on the brushes will be discussed in later sections.

**3.2.** Characterization of Cell Plasma Membrane Vesicles. Nanoparticle tracking analysis was employed to reveal the concentration, size, and polydispersity of cell plasma membrane vesicles made by the chemical-induction method. The concentration of cell membrane vesicles from our preparation methods was found to range as  $5.58 \times 10^8 \pm 3.02 \times 10^7$  particles/mL. The average size of the dominate peak in the tracking analysis for cell plasma membrane vesicles in these samples was 163.8 nm  $\pm 2.5$  nm, as shown in the particle size profile in Figure 3. Although the main peak of particle size is around 100-200 nm, the sample does contain some populations around 300 and 500 nm. Laser Doppler electrophoresis was used to measure the zeta-potential of the cell

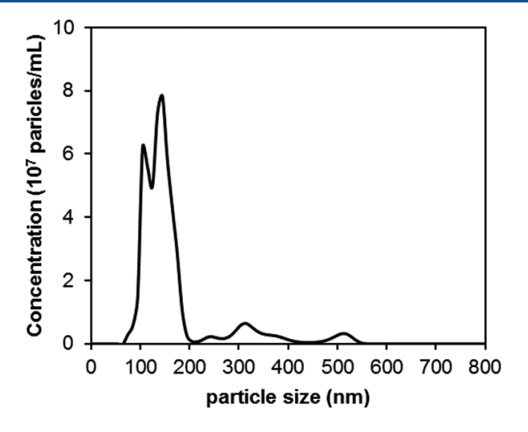


Figure 3. Particle size profile for cell plasma membrane vesicles generated using the chemical induction method.

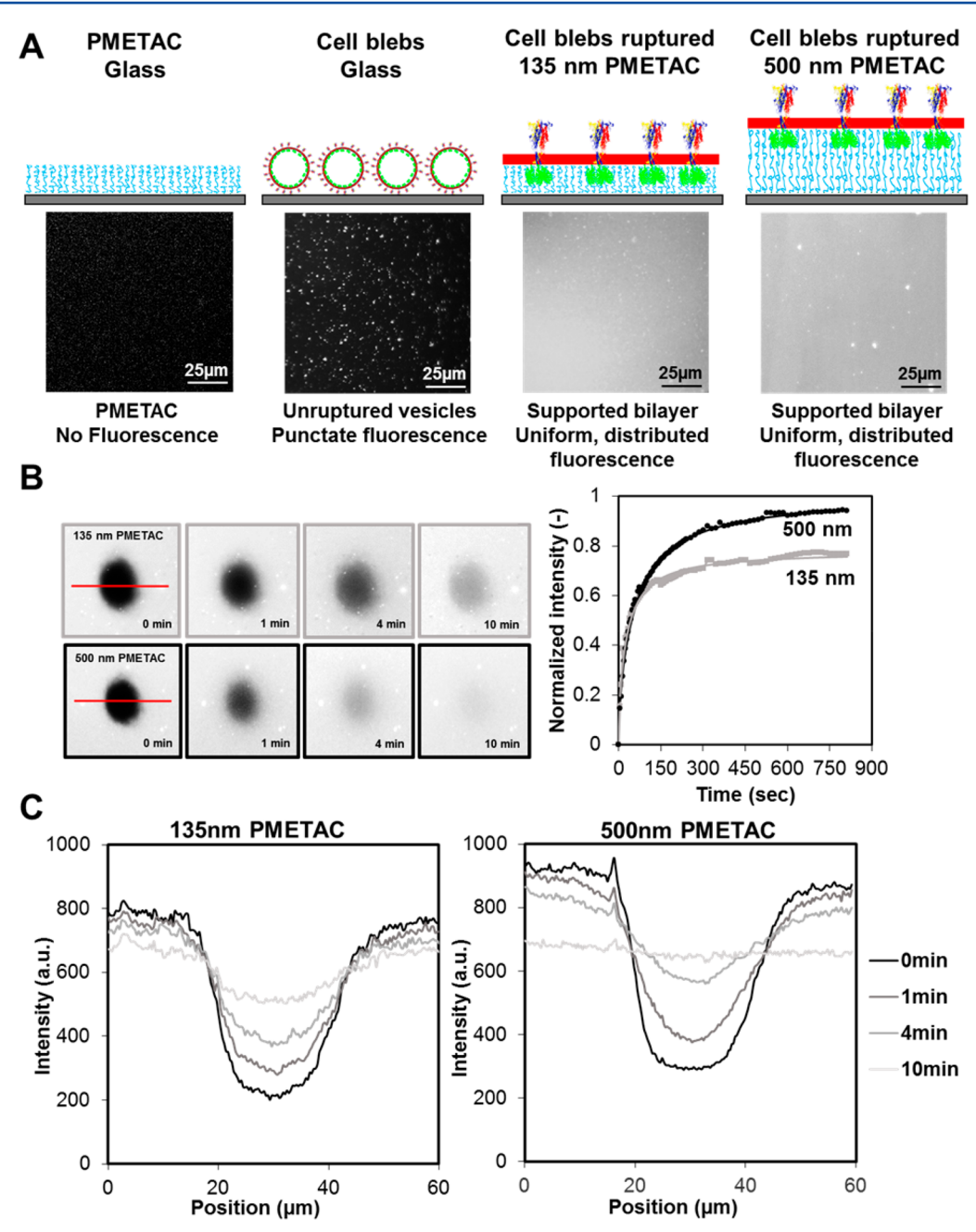


Figure 4. (A) A comparison of plain polymer cushion, blebs on plain glass, and blebs ruptured on PMETAC cushion, all at the same imaging conditions. (Left) The PMETAC brush does not contain any auto fluorescence signal. (Middle) Plasma cell membrane vesicles containing R18 adsorbed on glass slides do not rupture into a bilayer and R18 remains isolated within the vesicles. (Right) For the 500 nm PMETAC brush case, plasma membrane bilayer formed after incubating with the plasma cell membrane vesicles for 50 min shows uniform distribution of fluorescence. (B) After photobleaching, the recovery of bilayer is observed in the images. Diffusivity and mobile fractions of plasma membrane bilayers on both cushions, obtained by FRAP. (C) Line scans (taken from red lines in images in B) across the photobleaching spot show the intensity recovery over time.

plasma membrane vesicles. The zeta-potential of cell plasma membrane vesicles was around -12 mV in GPMV buffer.

The vesiculation process of forming cell plasma membrane vesicles involves formaldehyde and DTT and may have an impact on the composition of the cell plasma membrane vesicles produced. It is important to note that formaldehyde is a typical nonspecific cross-linking reagent (at much higher concentrations than used here; 4% vs 0.075%) and that DTT may reduce disulfide bonds and palmitoylated cysteines, which may impact protein phase partitioning<sup>21,65</sup> Furthermore, the chemical-induction treatment has been found to alter the

composition of cell plasma membrane vesicle and phase behavior, as reported in previous literature. Therefore, it is still unknown to what degree the cell plasma membrane vesicles generated by chemical-induction possess the full diversity of membrane species of the original cell plasma membrane. However, we confirm in later sections that the protein species we transfect in and are expressed in the plasma membrane of the cell are captured in the vesicles and wind up in the resulting planar bilayer, which is the primary objective of using this technique.

#### 3.3. Mobility in Supported Plasma Membrane Bilayer.

FRAP was employed to determine the overall lipid fluidity in the plasma membrane bilayer. R18 that has been incorporated into the membrane is the reporter for lipid mobility and formation of bilayer. Cell plasma membrane vesicles labeled with R18 were incubated in a well on PMETAC brushes or plain glass slides for 50 min. For vesicles adsorbed on glass slides with no cushion, the R18 signal remained confined in the plasma cell membrane vesicles, indicating no bilayer formation (Figure 4A). For both PMETAC brush lengths, 135 and 500 nm, the R18 was no longer confined in the cell blebs. The fluorescent images show the R18 spreads out relatively uniformly within the planar bilayer and supports the notion that a bilayer has formed (Figure 4A). Furthermore, after the bilayers were formed, a laser beam was used to bleach a 20  $\mu m$ diameter spot in the bilayers. After photobleaching, fluorescence recovery from the edges of the spot is a further indication of planar bilayer formation. The line scans across the photobleached spots for each cushion type (Figure 4B) indicate the profile of recovery of intensity over time (Figure 4C). The recovery of the photobleached spot was analyzed to reveal the diffusion coefficient and mobile fraction of the bilayer (Figure

Next, we compare membrane mobility of bilayers supported on the two lengths of PMETAC brushes and PEGylated lipid spacers. The bilayer with PEGylated lipid spacers was created by using PEGylated lipid vesicles<sup>67,68</sup> to induce the rupture of plasma cell membrane vesicles.<sup>27</sup> Although the presence of the PEG spacer beneath the bilayer and its thickness is still debated and not yet experimentally verified, we assume that the thickness of the PEGylated spacer was around a couple of nanometers. By theory of De Gennes<sup>69</sup> and Marsh,<sup>70</sup> we might expect the globular diameter of a PEG brush to be around 6 nm at these conditions, thus we refer to the bilayer supported on PEGylated lipid spacer as "6 nm PEG brush". The values for the diffusivity and mobile fractions of the plasma membrane bilayer for these various conditions, as reported by the R18 probe, are listed in Table 1.

Table 1. Diffusivity and Mobile Fraction of Plasma Membrane Bilayer on Different Lengths of PMETAC Brush, As Reported by R18 Membrane Intercalating Fluorophore by FRAP<sup>a</sup>

| cushion type        | diffusivity $(\mu m^2/s)$ | mobile fraction (%) |
|---------------------|---------------------------|---------------------|
| glass               | N/A                       | N/A                 |
| 6 nm PEG brush      | $0.30 \pm 0.03$           | $95 \pm 7.0$        |
| 135 nm PMETAC brush | $0.262 \pm 0.12$          | $75 \pm 2.5$        |
| 500 nm PMETAC brush | $0.456 \pm 0.041$         | $93 \pm 8.0$        |
|                     |                           |                     |

<sup>a</sup>The PEGylated bilayer data cited here is from previous literature.<sup>27</sup>

The bilayer on the 500 nm PMETAC cushion has both higher diffusivity and mobile fraction compared to the 135 nm PMETAC cushion. Some possible explanations are that the length or chain mobility of the PMETAC brushes have an impact on bilayer formation and quality of final bilayer. PMETAC is a strong polyelectrolyte brush in this configuration and it has been shown that the stretching extent of a PMETAC chain is only proportional to its length. For thicker brushes synthesized by "graft-from" method, the chains present on the swollen surface are only the longer chains, with the number of them decreasing with thickness, as the polydispersity increases proportionally. Therefore, the swollen surface of the thicker

brushes may be composed fewer longer chains, which may enable their higher mobility compared to the thinner brushes. This higher chain mobility, in turn, may reduce the resistance for the diffusion of the lipids in the bilayer above it. This postulate is also supported by Tang et al.<sup>32</sup> who pointed out that the higher fluctuation of polymer supports plays a central role in vesicle rupture and promotes the formation of a bilayer. On the other hand, lower chain mobility of the thinner PMETAC brushes may lead to the presence of more unruptured cell membrane vesicles, which could translate to barriers to contiguous bilayer formation and lead to immobile membrane species.

3.4. P2X2-Neon and GPI-YFP Orientation in Planar Plasma Membrane Bilayer. Here, an established enzyme accessibility assay was used to identify protein orientations in planar plasma membrane bilayers. 27,74,75 In cells, the fluorescent domain of GPI-YFP is located on the extracellular side of cell membrane, and the fluorescent domain of P2X2neon is located on the cytosolic side of the cell membrane. The plasma cell membrane vesicles blebbed from cells have already been shown to preserve these proteins' orientations in a previous study.<sup>27</sup> Thrombin cleaves the N-terminal neon domain of P2X2-neon and proteinase K cleaves the YFP domain of GPI-YFP. We note that the activity of thrombin for cleaving the same P2X2-neon used here was verified in a previous study.  $^{27}$  These enzymes were used here to indicate the GPI-YFP and P2X2-neon orientation in planar plasma membrane bilayers on PMETAC cushions. 74-76 Through these cleavage experiments, the rupture orientation of plasma membrane vesicles, bottom-up or top-down, can be inferred.

In the assay, the fluorescent signals from GPI-YFP and P2X2neon were monitored using variable angle epifluorescence microscopy instead of TIRF mode, due to the thickness of the polymer layers extending beyond TIRF range. For variable angle epifluorescence microscopy, at an oblique incident laser angle, the light was refracted so that the field of illumination was still narrow, providing high signal noise ratio for visualizing single fluorescent proteins within the planar bilayer. Just as in TIRF mode, as the fluorescent domain of proteins are cleaved by enzymes, the cleaved portion floats out of the illumination field, and the fluorescent signals at the bilayer surface decrease. Images were recorded at 10 min intervals for 30 min when intensity no longer changed substantially, indicating cleavage was complete. Typical microscopic images of fluorescent protein in bilayer are shown as examples in Figure 5. Before the enzyme treatment, either GPI-YFP or P2X2-neon signals are present (Figure 5A,C). After the enzyme treatment for 30 min, most of GPI-YFP signals are gone, but the bilayer still preserved significant signals from P2X2-neon (Figure 5B,D).

Each GPI-YFP or P2X2-neon signal in the images was tracked and counted to establish the signal loss or constant over time. As shown in Figure 5E,F, control cases were the GPI-YFP in plasma membrane bilayer without proteinase K treatment and P2X2-neon in plasma membrane bilayer without thrombin treatment, where the GPI-YFP and P2X2-neon signals remain unchanged over time (except for photobleaching). With proteinase K treatment, the bilayer has prominent drops in GPI-YFP signals for both PMETAC brushes. However, with thrombin treatment, the bilayer still maintains the P2X2-neon signals for both PMETAC brush case (except for some photobleaching), presumably because the enzyme cannot access the cleavage site beneath the bilayer. The results indicate that GPI-YFPs are facing up (outward toward the bulk) and

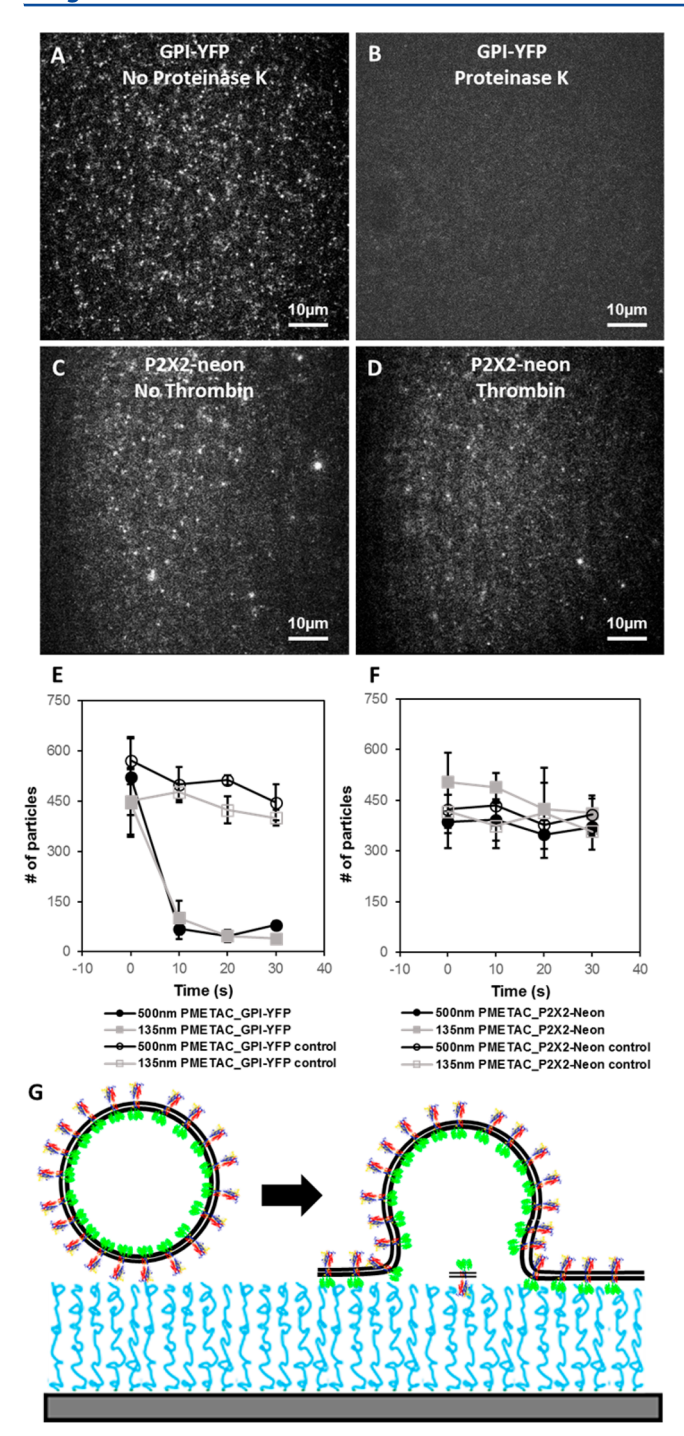


Figure 5. Enzyme accessibility assays for protein orientation in bilayer. The typical VAEM images of fluorescent protein in a bilayer on a 500 nm PMETAC brush are shown as follows: (A) GPI-YFP signals in bilayer before proteinase K treatment. (B) GPI-YFP signals in bilayer after 30 min of proteinase K treatment. (C) P2X2-neon signals in bilayer before thrombin treatment. (D) P2X2-neon signals in bilayer after 30 min of thrombin treatment. (E) GPI-YFP protein cleavage over time. At t = 0, Proteinase K was added to the well and cleaved all the accessible proteins. The signal drops indicate the GPI-YFP in bilayer was readily accessible (facing toward the bulk) for proteases. (F) P2X2-neon protein cleavage over time. At t = 0, thrombin was added to the bilayer to cleave all the accessible proteins. The signals remain, indicating that the P2X2-neon in bilayer was inaccessible for proteases (facing toward the polymer support). (G) Cartoon of the rupture process supported by the cleavage results: cell plasma membrane vesicles rupture as parachutes.

P2X2-neons are facing down (that is the neon tag is oriented facing downward toward the support) in the planar bilayers for both PMETAC brushes, just as has been shown for these proteins in PEGylated cushions in a previous study.<sup>27</sup> These results show that in both PMETAC brush cases, the GPI-YFP and P2X2-neon protein orientations are maintained as in live cells. These results imply the cell plasma membrane vesicles rupture like parachutes<sup>8,77</sup> on PMETAC, which keeps the luminal sides downward facing the cushion when the bilayer forms, and that this rupture mechanism seems to be preserved regardless of the length of PMETAC brush. (Figure 5G).

In the previous literature, <sup>78</sup> however, SLB formation by giant unilamellar vesicles was also studied and appears to invert the lipid leaflets (inside facing up toward the bulk aqueous phase). In this case, one would expect flipped protein orientation relative to what we observe here. One reason for the difference in rupture mechanism is that the size of giant unilamellar vesicles is larger than 1  $\mu$ m, significantly larger than the cell plasma membrane vesicles used here, which range from 100 to 500 nm. Furthermore, the substrate used in this work is a cationic polymer brush, which leads to electrostatic interaction with the cell plasma membrane vesicles, and may also further bias the rupture here in the "outside up" parachute-like orientation, although exactly how this might occur is still unknown and for future investigation.

Although the enzyme accessibility assay indicates cell plasma membrane vesicles rupture like parachutes and the orientation of the exogenously expressed proteins, GPI-YFP and P2X2-neon, in the resultant planar-supported lipid bilayer on the positivity-charged PMETAC brush are preserved as in the intact cell membrane, it is possible that other negatively charged membrane species could be reorganized and preferentially positioned in the bottom leaflet during the SLB formation, <sup>79,80</sup> as has been observed in other studies. Additional experiments are required to determine the orientation of other membrane species (such as negatively charged lipids and endogenous membrane proteins), to fully characterize the SLB formation on PMETAC brush.

**3.5. Single Particle Tracking of Membrane Protein Motion.** In this study, we investigated the motion of peripheral glycophospotidylinositol (GPI-linked) protein and a multipass transmembrane protein (P2X2). The motion of GPI-YFP and P2X2-neon in bilayers was examined by single particle tracking. Quantitative protein motion studies by mean squared displacement (MSD) analysis uses the initial slope of first three time steps to reveal the homogeneous diffusion constant. Moment scaling spectrum (MSS) analysis was used to assess the confinement of GPI-YFP and P2X2-neon in planar bilayers. <sup>58,62</sup>

In single particle tracking analysis, trajectories of single GPI-YFP and P2X2-neon were found by using a cost-minimized function to identify the location and intensity and then optimize the mapping process of GPI-YFP and P2X2-neon from frame to frame. Some typical tracking trajectories of GPI-YFP and P2X2-neon are shown in Figure 6.

The diffusion coefficient, mobile fraction, and percent confinement for each protein type are provided in Table 2, comparing the various bilayer support systems. The first point to notice is that the GPI-link proteins on all surfaces (except plain glass, which do not form bilayers) are all about the same for each of the three parameters. Because this type of protein is located on the uppermost leaflet facing the bulk, it is not surprising that the values are not much impacted by the

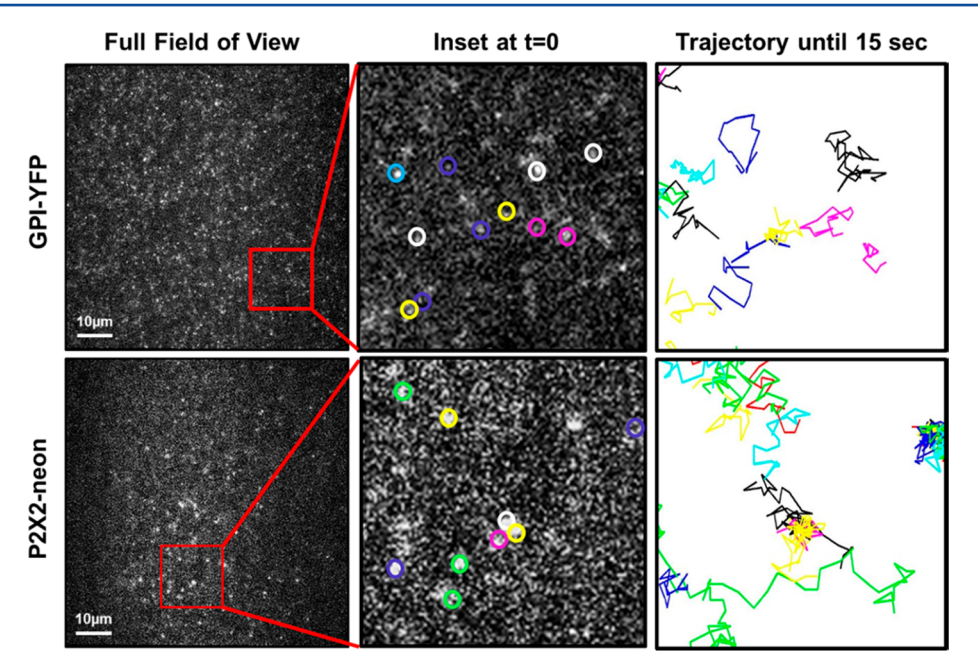


**Figure 6.** Typical trajectory of GPI-YFP and P2X2-neon in bilayer on 500 nm PMETAC brush. (Left) Full field of view and (middle) inset of first frame were shown to reveal the start point of fluorescent protein (circled in corresponding colors). The trajectories of fluorescent protein tracked for 15 s are shown to reveal the protein diffusion in the 2D plane.

Table 2. Comparison of GPI-YFP and P2X2-Neon Mobility, Diffusivity, and Confinement in PEGylated Bilayer on Glass Slides and Plasma Membrane Bilayer on Different Lengths of PMETAC Brush

| GPI-YFP                        | mobility (%)   | diffusion coefficient $(\mu m^2/s)$ | confinement (%) |
|--------------------------------|----------------|-------------------------------------|-----------------|
| PEGylated bilayer              | $86.3 \pm 5.1$ | $0.680 \pm 0.236$                   | $66.7 \pm 4.7$  |
| 135 nm<br>PMETAC               | $69.3 \pm 8.0$ | $0.536 \pm 0.221$                   | $75.0 \pm 1.9$  |
| 500 nm<br>PMETAC               | $91.0 \pm 4.6$ | $0.671 \pm 0.253$                   | $63.5 \pm 4.6$  |
|                                |                |                                     |                 |
| P2X2-neon                      | mobility (%)   | diffusion coefficient $(\mu m^2/s)$ | confinement (%) |
| P2X2-neon<br>PEGylated bilayer |                |                                     |                 |
|                                | (%)            | $(\mu \text{m}^2/\text{s})$         | (%)             |

support. Interestingly, this protein type is also suspected to be located in lipid rafts in cells, and given that the confinement percentage also does not change among the support systems, it seems to suggest that the confinement we observe is reflective of the membrane heterogeneity present in the bilayer and not an effect of the support.

The situation is different for the P2X2 transmembrane proteins. \$1,82 Here there is a clear trend in increasing diffusivity coefficient, mobile fraction, and reduction in confinement as the cushion thickness increases, suggesting the confinement observed results in part from the support interactions and that these are minimized with larger cushions. The P2X2-neon in bilayers on 500 nm PMETAC brush possesses ~25% more protein mobility, ~ 34% increase in diffusion coefficient, and ~20% lower protein confinement compared to the PEGylated bilayer on glass slides (Table 2). It is of particular note that the PEGylated bilayers are significantly diluted with extra lipids from the fusogenic vesicles that mix with the plasma membrane constituents when the bilayer forms, while the bilayers formed

on PMETAC are from purely plasma membrane blebs, thus the comparison of diffusion values is not quite fair because the protein concentration in PEGylated bilayers is more dilute. However, this feature makes the results on PMETAC cushions even more significant, when considering there is significantly more protein in PMETAC bilayers, yet the diffusion is less hindered and confined compared to the PEGylated bilayers.

The above analysis of the cationic PMETAC brushes illustrates that these cushions can induce the formation of bilayers from plasma cell membrane vesicles and preserve the orientation and mobility of membrane proteins expressed in them. However, single particle tracking analysis still shows an immobile fraction of membrane protein in both PMETAC brush conditions. A possible explanation is the drag/tangling of the cytosolic portion of the protein interacting with the PMETAC chain network. Additionally, in a plasma membrane bilayer, negatively charged domains of proteins and lipids may stick to the cationic polymer brush electrostatically. The remaining possibility is that there are defects or unruptured vesicles present in the surface.

#### 4. CONCLUSIONS

Planar cell plasma membrane bilayers were created from native cell plasma membrane vesicles by leveraging the electrostatic interaction between the polyelectrolyte brush and the oppositely charged membrane vesicles. To our knowledge, this is the first planar bilayer platform created directly from cell plasma membrane vesicles, without dilution by any synthetic liposomes, while demonstrating significantly higher mobility of integral transmembrane proteins and preserving their native orientation. Because of these features, this platform represents the cell plasma membrane surface more closely and may be advantageous for *in vitro* models and assays used to study phenomena in a variety of biological research areas, including studies of host cell—pathogen interactions, cell—cell organization in tissue engineering, or the development of abiotic/ biotic interfaces, to name a few.

#### ASSOCIATED CONTENT

#### **S** Supporting Information

The Supporting Information is available free of charge on the ACS Publications website at DOI: 10.1021/acs.langmuir.7b02945.

Full descriptions of Movies 1 and 2 (PDF) GPI-YFP on 500 nm PMETAC cushion (AVI) P2X2-Neon on 500 nm PMETAC cushion (AVI)

#### AUTHOR INFORMATION

#### ORCID ®

Han-Yuan Liu: 0000-0002-9398-6969 Wei-Liang Chen: 0000-0003-2581-1996 Susan Daniel: 0000-0001-7773-0835

## Author Contributions §Contributed equally

#### **Notes**

The authors declare no competing financial interest.

#### ACKNOWLEDGMENTS

The authors would like to thank Barbara Baird and David Holowka of Cornell University for providing the pYFP-GPI-N1 plasmid and Toshi Kawate of Cornell University for providing the pINR3-Neon-THR-P2X2 plasmid. This work was supported in part by the following grants to C.O.: National Science Foundation (CHE-1709660). This work was supported in part by the following grants to S.D.: Memorial Sloan Kettering Cancer Center U54CA199081 subaward BD520101. This work made use of the Cornell Center for Materials Research Shared Facilities, which are supported through the NSF MRSEC program (DMR-1120296).

#### REFERENCES

- (1) Qi, S.; Groves, J. T.; Chakraborty, A. K. Synaptic pattern formation during cellular recognition. *Proc. Natl. Acad. Sci. U. S. A.* **2001**, 98 (12), 6548–6553.
- (2) Kholodenko, B. N. Cell-signalling dynamics in time and space. *Nat. Rev. Mol. Cell Biol.* **2006**, *7* (3), 165–176.
- (3) Saftig, P.; Klumperman, J. Lysosome biogenesis and lysosomal membrane proteins: Trafficking meets function. *Nat. Rev. Mol. Cell Biol.* **2009**, *10* (9), 623–635.
- (4) Sandermann, H. Regulation of membrane enzymes by lipids. *Biochim. Biophys. Acta, Rev. Biomembr.* **1978**, *515* (3), 209–237.
- (5) Lingwood, D.; Simons, K. Lipid rafts as a membrane-organizing principle. *Science* **2010**, 327 (5961), 46–50.
- (6) Gamper, N.; Shapiro, M. S. Regulation of ion transport proteins by membrane phosphoinositides. *Nat. Rev. Neurosci.* **2007**, 8 (12), 921–934.
- (7) Costello, D. A.; Millet, J. K.; Hsia, C.-Y.; Whittaker, G. R.; Daniel, S. Single particle assay of coronavirus membrane fusion with proteinaceous receptor-embedded supported bilayers. *Biomaterials* **2013**, 34 (32), 7895–7904.
- (8) Hsia, C.-Y.; Chen, L.; Singh, R. R.; DeLisa, M. P.; Daniel, S. A Molecularly Complete Planar Bacterial Outer Membrane Platform. *Sci. Rep.* **2016**, *6*, 32715.
- (9) Hsia, C.-Y.; Richards, M. J.; Daniel, S. A review of traditional and emerging methods to characterize lipid—protein interactions in biological membranes. *Anal. Methods* **2015**, *7* (17), 7076—7094.
- (10) Konopka, C. A.; Bednarek, S. Y. Variable-angle epifluorescence microscopy: a new way to look at protein dynamics in the plant cell cortex. *Plant J.* **2008**, *53* (1), 186–196.
- (11) Langhans, M.; Meckel, T. Single-molecule detection and tracking in plants. *Protoplasma* **2014**, *251* (2), 277–291.

(12) Wan, Y.; Ash, W. M.; Fan, L.; Hao, H.; Kim, M. K.; Lin, J. Variable-angle total internal reflection fluorescence microscopy of intact cells of Arabidopsis thaliana. *Plant Methods* **2011**, *7* (1), 27.

- (13) Kalb, E.; Engel, J.; Tamm, L. K. Binding of Proteins to Specific Target Sites in Membranes Measured by Total Internal Reflection Fluorescence Microscopy. *Biochemistry* **1990**, *29*, 1607–1613.
- (14) Watts, T. H.; Gaub, H. E.; McConnell, H. M. T-cell-mediated association of peptide antigen and major histocompatibility complex protein detected by energy transfer in an evanescent wave-field. *Nature* 1986, 320, 179–181.
- (15) Chiantia, S.; Ries, J.; Kahya, N.; Schwille, P. Combined AFM and Two-Focus SFCS Study of Raft-Exhibiting Model Membranes. *ChemPhysChem* **2006**, *7* (11), 2409–2418.
- (16) Richter, R. P.; Brisson, A. R. Following the Formation of Supported Lipid Bilayers on Mica: A Study Combining AFM, QCM-D, and Ellipsometry. *Biophys. J.* **2005**, 88 (5), 3422–3433.
- (17) Cho, N.-J.; Frank, C. W.; Kasemo, B.; Höök, F. Quartz crystal microbalance with dissipation monitoring of supported lipid bilayers on various substrates. *Nat. Protoc.* **2010**, *5* (6), 1096–1106.
- (18) Murray, D. T.; Griffin, J.; Cross, T. A. Detergent optimized membrane protein reconstitution in liposomes for solid state NMR. *Biochemistry* **2014**, *53* (15), 2454–2463.
- (19) Grillitsch, K.; Tarazona, P.; Klug, L.; Wriessnegger, T.; Zellnig, G.; Leitner, E.; Feussner, I.; Daum, G. Isolation and characterization of the plasma membrane from the yeast Pichia pastoris. *Biochim. Biophys. Acta, Biomembr.* **2014**, *1838* (7), 1889–1897.
- (20) Tanaka, M.; Rossetti, F. F.; Kaufmann, S. Native supported membranes: creation of two-dimensional cell membranes on polymer supports. *Biointerphases* **2008**, *3* (2), FA12–FA16.
- (21) Sezgin, E.; Kaiser, H.-J.; Baumgart, T.; Schwille, P.; Simons, K.; Levental, I. Elucidating membrane structure and protein behavior using giant plasma membrane vesicles. *Nat. Protoc.* **2012**, *7* (6), 1042.
- (22) Baumgart, T.; Hammond, A. T.; Sengupta, P.; Hess, S. T.; Holowka, D. A.; Baird, B. A.; Webb, W. W. Large-scale fluid/fluid phase separation of proteins and lipids in giant plasma membrane vesicles. *Proc. Natl. Acad. Sci. U. S. A.* **2007**, *104* (9), 3165–3170.
- (23) Scott, R. E. Plasma membrane vesiculation: A new technique for isolation of plasma membranes. *Science* **1976**, *194*, 743–745.
- (24) Tanaka, M.; Kaufmann, S.; Nissen, J.; Hochrein, M. Orientation selective immobilization of human erythrocyte membranes on ultrathin cellulose films. *Phys. Chem. Chem. Phys.* **2001**, 3 (18), 4091–4095.
- (25) Simonsson, L.; Gunnarsson, A.; Wallin, P.; Jönsson, P.; Höök, F. Continuous lipid bilayers derived from cell membranes for spatial molecular manipulation. *J. Am. Chem. Soc.* **2011**, *133* (35), 14027–14032.
- (26) Pace, H.; Simonsson Nyström, L.; Gunnarsson, A.; Eck, E.; Monson, C.; Geschwindner, S.; Snijder, A.; Höök, F. Preserved transmembrane protein mobility in polymer-supported lipid bilayers derived from cell membranes. *Anal. Chem.* **2015**, *87* (18), 9194–9203.
- (27) Richards, M. J.; Hsia, C.-Y.; Singh, R. R.; Haider, H.; Kumpf, J.; Kawate, T.; Daniel, S. Membrane protein mobility and orientation preserved in supported bilayers created directly from cell plasma membrane blebs. *Langmuir* **2016**, *32* (12), 2963–2974.
- (28) Brian, A. A.; McConnell, H. M. Allogeneic stimulation of cytotoxic T cells by supported planar membranes. *Proc. Natl. Acad. Sci. U. S. A.* **1984**, *81* (19), 6159–6163.
- (29) Tamm, L. K.; McConnell, H. M. Supported phospholipid bilayers. *Biophys. J.* **1985**, *47* (1), 105–113.
- (30) König, B. W.; Krueger, S.; Orts, W.; Majkrzak, C. F.; Berk, N. F.; Silverton, J.; Gawrisch, K. Neutron reflectivity and atomic force microscopy studies of a lipid bilayer in water adsorbed to the surface of a silicon single crystal. *Langmuir* **1996**, *12* (5), 1343–1350.
- (31) Andersson, J.; Köper, I. Tethered and polymer supported bilayer lipid membranes: Structure and function. *Membranes* **2016**, 6 (2), 30.
- (32) Tang, Y.; Wang, Z.; Xiao, J.; Yang, S.; Wang, Y. J.; Tong, P. Studies of phospholipid vesicle deposition/transformation on a polymer surface by dissipative quartz crystal microbalance and atomic force microscopy. *J. Phys. Chem. B* **2009**, *113* (45), 14925–14933.

(33) Knoll, W.; Frank, C.; Heibel, C.; Naumann, R.; Offenhäusser, A.; Rühe, J.; Schmidt, E.; Shen, W.; Sinner, A. Functional tethered lipid bilayers. *Rev. Mol. Biotechnol.* **2000**, *74* (3), 137–158.

- (34) Renner, L.; Pompe, T.; Lemaitre, R.; Drechsel, D.; Werner, C. Controlled enhancement of transmembrane enzyme activity in polymer cushioned supported bilayer membranes. *Soft Matter* **2010**, 6 (21), 5382–5389.
- (35) Smith, E. A.; Coym, J. W.; Cowell, S. M.; Tokimoto, T.; Hruby, V. J.; Yamamura, H. I.; Wirth, M. J. Lipid bilayers on polyacrylamide brushes for inclusion of membrane proteins. *Langmuir* **2005**, *21* (21), 9644–9650.
- (36) Ma, C.; Srinivasan, M.; Waring, A. J.; Lehrer, R. I.; Longo, M. L.; Stroeve, P. Supported lipid bilayers lifted from the substrate by layer-by-layer polyion cushions on self-assembled monolayers. *Colloids Surf., B* **2003**, *28* (4), 319–329.
- (37) Zhang, L.; Vidu, R.; Waring, A. J.; Lehrer, R. I.; Longo, M. L.; Stroeve, P. Electrochemical and surface properties of solid-supported, mobile phospholipid bilayers on a polyion/alkylthiol layer pair used for detection of antimicrobial peptide insertion. *Langmuir* **2002**, *18* (4), 1318–1331.
- (38) Chen, W.-L.; Cordero, R.; Tran, H.; Ober, C. K. 50th Anniversary Perspective: Polymer Brushes: Novel Surfaces for Future Materials. *Macromolecules* **2017**, *50*, 4089.
- (39) Zhou, Z.; Yu, P.; Geller, H. M.; Ober, C. K. Biomimetic polymer brushes containing tethered acetylcholine analogs for protein and hippocampal neuronal cell patterning. *Biomacromolecules* **2013**, *14* (2), 529–537.
- (40) Meng, J.; Cao, Z.; Ni, L.; Zhang, Y.; Wang, X.; Zhang, X.; Liu, E. A novel salt-responsive TFC RO membrane having superior antifouling and easy-cleaning properties. *J. Membr. Sci.* **2014**, *461*, 123–129.
- (41) Faulón Marruecos, D.; Kastantin, M.; Schwartz, D. K.; Kaar, J. L. Dense Poly (ethylene glycol) Brushes Reduce Adsorption and Stabilize the Unfolded Conformation of Fibronectin. *Biomacromolecules* **2016**, *17* (3), 1017–1025.
- (42) Welch, M.; Rastogi, A.; Ober, C. Polymer brushes for electrochemical biosensors. *Soft Matter* **2011**, *7* (2), 297–302.
- (43) Cheng, N.; Bao, P.; Evans, S.; Leggett, G.; Armes, S. Facile formation of highly mobile supported lipid bilayers on surface-quaternized pH-responsive polymer brushes. *Macromolecules* **2015**, *48* (9), 3095–3103.
- (44) Kaufmann, M.; Jia, Y.; Werner, C.; Pompe, T. Weakly coupled lipid bilayer membranes on multistimuli-responsive poly (n-isopropylacrylamide) copolymer cushions. *Langmuir* **2011**, 27 (2), 513–516.
- (45) Santonicola, M. G.; Memesa, M.; Meszyńska, A.; Ma, Y.; Vancso, G. J. Surface-grafted zwitterionic polymers as platforms for functional supported phospholipid membranes. *Soft Matter* **2012**, 8 (5), 1556–1562.
- (46) Blakeston, A. C.; Alswieleh, A. M.; Heath, G. R.; Roth, J. S.; Bao, P.; Cheng, N.; Armes, S. P.; Leggett, G. J.; Bushby, R. J.; Evans, S. D. New poly (amino acid methacrylate) brush supports the formation of well-defined lipid membranes. *Langmuir* **2015**, *31* (12), 3668–3677.
- (47) Dunlop, I. E.; Thomas, R. K.; Titmus, S.; Osborne, V.; Edmondson, S.; Huck, W. T.; Klein, J. Structure and collapse of a surface-grown strong polyelectrolyte brush on sapphire. *Langmuir* **2012**, 28 (6), 3187–3193.
- (48) Ramos, J. J. I.; Moya, S. E. Water content of hydrated polymer brushes measured by an in situ combination of a quartz crystal microbalance with dissipation monitoring and spectroscopic ellipsometry. *Macromol. Rapid Commun.* **2011**, 32 (24), 1972–1978.
- (49) Dong, R.; Molloy, R. P.; Lindau, M.; Ober, C. K. Direct synthesis of quaternized polymer brushes and their application for guiding neuronal growth. *Biomacromolecules* **2010**, *11* (8), 2027–2032.
- (50) Kawate, T.; Michel, J. C.; Birdsong, W. T.; Gouaux, E. Crystal structure of the ATP-gated P2 × 4 ion channel in the closed state. *Nature* **2009**, 460 (7255), 592–598.

(51) Koepsel, R. R.; Russell, A. J.; Ravikumar, T. Methods, devices and systems for biocidal surface activity. U.S. Patent Application 20090074709 A1, 2009.

- (52) Ramakrishnan, A.; Dhamodharan, R.; Rühe, J. Controlled growth of PMMA brushes on silicon surfaces at room temperature. *Macromol. Rapid Commun.* **2002**, 23 (10–11), 612–616.
- (53) Zhang, T.; Du, Y.; Müller, F.; Amin, I.; Jordan, R. Surface-initiated Cu (0) mediated controlled radical polymerization (SI-CuCRP) using a copper plate. *Polym. Chem.* **2015**, *6* (14), 2726–2733.
- (54) Soumpasis, D. Theoretical analysis of fluorescence photobleaching recovery experiments. *Biophys. J.* **1983**, *41* (1), 95–97.
- (55) Vrljic, M.; Nishimura, S. Y.; Moerner, W. Single-molecule tracking. *Methods Mol. Biol.* **2007**, 398, 193–219.
- (56) Sonnleitner, A.; Schütz, G.; Schmidt, T. Free Brownian motion of individual lipid molecules in biomembranes. *Biophys. J.* **1999**, 77 (5), 2638–2642.
- (57) Poudel, K. R.; Jones, J. P.; Brozik, J. A. A guide to tracking single transmembrane proteins in supported lipid bilayers. *Methods Mol. Biol.* **2013**, *974*, 233–252.
- (58) Ferrari, R.; Manfroi, A.; Young, W. Strongly and weakly self-similar diffusion. *Phys. D* **2001**, *154* (1), 111–137.
- (59) Smith, M. B.; Karatekin, E.; Gohlke, A.; Mizuno, H.; Watanabe, N.; Vavylonis, D. Interactive, computer-assisted tracking of speckle trajectories in fluorescence microscopy: application to actin polymerization and membrane fusion. *Biophys. J.* **2011**, *101* (7), 1794–1804.
- (60) Smith, P. R.; Morrison, I. E.; Wilson, K. M.; Fernandez, N.; Cherry, R. J. Anomalous diffusion of major histocompatibility complex class I molecules on HeLa cells determined by single particle tracking. *Biophys. J.* **1999**, *76* (6), 3331–3344.
- (61) Kusumi, A.; Sako, Y.; Yamamoto, M. Confined lateral diffusion of membrane receptors as studied by single particle tracking (nanovid microscopy). Effects of calcium-induced differentiation in cultured epithelial cells. *Biophys. J.* **1993**, 65 (5), 2021–2040.
- (62) Sbalzarini, I. F.; Koumoutsakos, P. Feature point tracking and trajectory analysis for video imaging in cell biology. *J. Struct. Biol.* **2005**, *151* (2), 182–195.
- (63) Anastasaki, A.; Nikolaou, V.; Nurumbetov, G.; Wilson, P.; Kempe, K.; Quinn, J. F.; Davis, T. P.; Whittaker, M. R.; Haddleton, D. M. Cu (0)-mediated living radical polymerization: a versatile tool for materials synthesis. *Chem. Rev.* **2016**, *116* (3), 835–877.
- (64) Boyer, C.; Soeriyadi, A. H.; Zetterlund, P. B.; Whittaker, M. R. Synthesis of complex multiblock copolymers via a simple iterative Cu (0)-mediated radical polymerization approach. *Macromolecules* **2011**, 44 (20), 8028–8033.
- (65) Levental, I.; Lingwood, D.; Grzybek, M.; Coskun, Ü.; Simons, K. Palmitoylation regulates raft affinity for the majority of integral raft proteins. *Proc. Natl. Acad. Sci. U. S. A.* **2010**, *107* (51), 22050–22054.
- (66) Levental, I.; Grzybek, M.; Simons, K. Raft domains of variable properties and compositions in plasma membrane vesicles. *Proc. Natl. Acad. Sci. U. S. A.* **2011**, *108* (28), 11411–11416.
- (67) Albertorio, F.; Daniel, S.; Cremer, P. S. Supported lipopolymer membranes as nanoscale filters: simultaneous protein recognition and size selection assays. *J. Am. Chem. Soc.* **2006**, *128*, 7168–7169.
- (68) Diaz, A. J.; Albertorio, F.; Daniel, S.; Cremer, P. S. Double cushions preserve transmembrane protein mobility in supported bilayer systems. *Langmuir* **2008**, 24, 6820–6826.
- (69) De Gennes, P.-G. Scaling Concepts in Polymer Physics; Cornell University Press: Ithaca, NY, 1979.
- (70) Marsh, D.; Bartucci, R.; Sportelli, L. Lipid membranes with grafted polymers: physicochemical aspects. *Biochim. Biophys. Acta, Biomembr.* **2003**, *1615* (1–2), 33–59.
- (71) Biesalski, M.; Rühe, J. Scaling laws for the swelling of neutral and charged polymer brushes in good solvents. *Macromolecules* **2002**, 35 (2), 499–507.
- (72) Martinez, A. P.; Carrillo, J.-M. Y.; Dobrynin, A. V.; Adamson, D. H. Distribution of Chains in Polymer Brushes Produced by a "Grafting From" Mechanism. *Macromolecules* **2016**, *49* (2), 547–553.
- (73) Patil, R. R.; Turgman-Cohen, S.; Šrogl, J. í.; Kiserow, D.; Genzer, J. On-demand degrafting and the study of molecular weight

and grafting density of poly (methyl methacrylate) brushes on flat silica substrates. *Langmuir* **2015**, *31* (8), 2372–2381.

- (74) Fischer, F.; Poetsch, A. Protein cleavage strategies for an improved analysis of the membrane proteome. *Proteome Sci.* **2006**, *4* (1), 2.
- (75) Wu, C. C.; MacCoss, M. J.; Howell, K. E.; Yates, J. R. A method for the comprehensive proteomic analysis of membrane proteins. *Nat. Biotechnol.* **2003**, *21* (5), 532–538.
- (76) Lorenz, H.; Hailey, D. W.; Wunder, C.; Lippincott-Schwartz, J. The fluorescence protease protection (FPP) assay to determine protein localization and membrane topology. *Nat. Protoc.* **2006**, *1* (1), 276.
- (77) Fuhrmans, M.; Muller, M. Mechanisms of vesicle spreading on surfaces: coarse-grained simulations. *Langmuir* **2013**, 29 (13), 4335–4349
- (78) Hamai, C.; Cremer, P. S.; Musser, S. M. Single giant vesicle rupture events reveal multiple mechanisms of glass-supported bilayer formation. *Biophys. J.* **2007**, 92 (6), 1988–1999.
- (79) Käsbauer, M.; Junglas, M.; Bayerl, T. M. Effect of Cationic Lipids in the Formation of Asymmetries in Supported Bilayers. *Biophys. J.* **1999**, *76* (5), 2600–2605.
- (80) Shreve, A. P.; Howland, M. C.; Sapuri-Butti, A. R.; Allen, T. W.; Parikh, A. N. Evidence for Leaflet-Dependent Redistribution of Charged Molecules in Fluid Supported Phospholipid Bilayers. *Langmuir* **2008**, 24 (23), 13250–13253.
- (81) Allsopp, R. C.; Lalo, U.; Evans, R. J. Lipid Raft Association and Cholesterol Sensitivity of  $P2 \times 1-4$  Receptors for ATP Chimeras and Point Mutants Identify Intracellular Amino-terminal Residues Involved in Lipid Regulation of  $P2 \times 1$  Receptors. *J. Biol. Chem.* **2010**, 285 (43), 32770–32777.
- (82) Robinson, L. E.; Murrell-Lagnado, R. D. The trafficking and targeting of P2X receptors. Front. Cell. Neurosci. 2013, 7, 233.